ENCLOSURE 2

MFN 07-561

NEDO-33173, Supplement 2, Part 1
DRAFT

Non-Proprietary Version

IMPORTANT NOTICE

This is a non-proprietary version of Enclosure 1 to MFN 07-561, from which the proprietary information has been removed. Portions of the enclosure that have been removed are indicated by an open and closed bracket as shown here [[ ]]

HITACHI

GE Hitachi Nuclear Energy

NEDO-33173
Supplement 2, Part 1
Revision 0
Class I
eDRF-0000-0075-2554
October 2007

Licensing Topical Report

Power Distribution Validation for Cofrentes Cycle 13

DRAFT

DRAFT

INFORMATION NOTICE

This document is the GE Hitachi Nuclear Energy Americas (GEH) non-proprietary version of NEDC-33173P Supplement 2, Part 1 from which the proprietary information has been removed.

Portions of the document that have been removed are indicated by white space with open and closed double square brackets as shown here [[ ]].

IMPORTANT NOTICE REGARDING CONTENTS OF THIS REPORT

PLEASE READ CAREFULLY

The information contained in this document is furnished for the purpose of obtaining NRC approval of the Interim Methods approach and process to support Extended Power Uprate and Maximum Extended Load Line Limit Analysis Plus Applications. The only undertakings of GE Hitachi Nuclear Energy Americas LLC (GEH) with respect to information in this document are contained in contracts between GEH and participating utilities, and nothing contained in this document shall be construed as changing those contracts. The use of this information by anyone other than that for which it is intended is not authorized; and with respect to any unauthorized use, GEH makes no representation or warranty, and assumes no liability as to the completeness, accuracy, or usefulness of the information contained in this document.

Table of Contents

1 Introduction 1-1
2 Plant and Fuel Description 2-1
3 Traversing In-core Probe Comparisons 3-1
3.1 Definition of Statistics 3-1
3.2 TIP Summary 3-4
4 Gamma Scan Comparisons 4-1
4.1 Utilization of the Data for Power Distribution Benchmark 4-1
4.2 Considering Geometrical Effects on the Gamma Scan 4-2
4.3 Definition of Statistics and Process 4-3
4.4 Gamma Scan Comparison Summary 4-4
5 [[ ]] 5-1
5.1 Definition of Statistics 5-1
5.2 [[ ]] 5-1
6 Conclusions 6-1
7 References 7-1

List of Figures

Figure 2-1 Cycle 13 Loading Pattern 2-2
Figure 2-2 Cycle 13 Power/Flow History 2-3
Figure 3-1: Summary of PANAC11 TIP Comparisons 3-5
Figure 3-2: Summary of PANAC10 TIP Comparisons 3-5
Figure 3-3 Core Average TIP for TIP dated April 9, 2001 (PANAC11) 3-7
Figure 3-4 Detail of TIP dated April 9, 2001 (PANAC11) 3-7
Figure 3-5 Core Average TIP for TIP dated January 7, 2002 (47 days prior to shutdown, PANAC11) 3-8
Figure 3-6 Detail of TIP dated January 7, 2002 (47 days prior to shutdown, PANAC11) 3-8
Figure 3-7 Core Average TIP dated February 19, 2002 (4 days prior to shutdown, PANAC11) 3-9
Figure 3-8 Detail of TIP dated February 19, 2002 (4 days prior to shutdown, PANAC11) 3-9
Figure 4-1 Depiction of the fuel and collimator geometry (dimensions removed) 4-2
Figure 4-2 Comparison of Predicted vs. Measured Results (PANAC11) 4-7
Figure 4-3 Comparison of Predicted vs. Measured Results (PANAC10) 4-8
Figure 4-4 Error in Bundle Average ^{140}Ba versus Exposure (PANAC11) 4-9
Figure 4-5 Error in Bundle Average ^{140}Ba versus Exposure (PANAC10) 4-10
Figure 4-6 Error in Bundle Average ^{140}Ba versus Distance to Center (PANAC11) 4-11
Figure 4-7 Error in Bundle Average ^{140}Ba versus Distance to Center (PANAC10 4-12
Figure 4-8 Error in Bundle Average ^{140}Ba versus Distance to Center (PANAC11, all bundles) 4-13
Figure 4-9 Examination for Trending versus Bundle Power (PANAC11) 4-14
Figure 4-10 Examination of Trending versus Axial Height (PANAC11) 4-15
Figure 4-11 Examination of Trending versus Axial Height (PANAC11, Adaptive) 4-16
Figure 4-12 Bundle Average ^{140}Ba Error (Δ, PANAC11, Adaptive) –Left 4-17
Figure 4-13 Bundle Average ^{140}Ba Error (Δ, PANAC11, Adaptive) - Right 4-18
Figure 4-14 Bundle Average ^{140}Ba Error (Δ, PANAC10, Adaptive) - Left 4-19
Figure 4-15 Bundle Average ^{140}Ba Error (Δ, PANAC10, Adaptive) - Right 4-20
Figure 4-16 Bundle Average ^{140}Ba Error (%, PANAC11, Adaptive) -Left 4-21
Figure 4-17 Bundle Average ^{140}Ba Error (%, PANAC11, Adaptive) – Right 4-22
Figure 4-18 Bundle Average ^{140}Ba Error (%, PANAC10, Adaptive) –Left 4-23
Figure 4-19 Bundle Average ^{140}Ba Error (%, PANAC10, Adaptive) –Right 4-24
Figure 5-1 [[ ]] (PANAC11, Adaptive) -Left 5-4

Figure 5-2 [[ ]] (PANAC11, Adaptive) -Right 5-5
Figure 5-3 [[ ]] (PANAC10) - Left 5-6
Figure 5-4 [[ ]] (PANAC10) - Right.....5-7

List of Tables

Table 2-1 Fuel Composition of Cycle 13 2-1
Table 3-1 Summary of PANAC10 and PANAC11 TIP Comparisons 3-6
Table 4-1 Summary of Gamma Scan Comparison 4-5
Table 5-1 Summary of [[ ]] Comparisons 5-2
Table 5-2 Summary of Gamma Scan Measurements Using the PANAC10 3D Simulator 5-3
Table 5-3 Summary of Gamma Scan Measurements Using the PANAC11 3D Simulator 5-8

DRAFT

Abstract

Gamma scan is a non-destructive method to determine the relative fission product inventory in nuclear fuel. A gamma scan campaign was completed in 2002 at the Cofrentes Nuclear Power Plant. Fifty bundles were examined including multiple vendor 10x10 bundle designs. The agreement between the measurements and predictions using the TGBLA06 lattice physics code and the PANAC11 BWR core simulator is excellent, with radial RMS errors less than 2% at bundle level and less than 4% at a nodal level. The data validate the applicability of the assembly power uncertainty for modern core and fuel designs and operational strategies. Additional observations include confirmation of the consistency between validation using operational TIP data and the validation resulting from a gamma scan.

1 Introduction

Power distribution validation data for operating boiling water reactors is routinely taken in the form of traversing in-core probe (TIP) measurements. In this case, the average power of the four bundles surrounding the instrument tube is detected via a neutron sensitive or gamma sensitive detector. For potentially greater resolution and at greater effort and cost, gamma scanning is an additional non-destructive method to determine the relative fission product inventory and recent power history in BWR nuclear fuel bundles.

Gamma scan measurement programs vary by specification of the physical locality of the measurement, time from reactor shutdown to performance of the measurement, duration of the measurement, and number of measurements. For example, the technique for measurements of "power" calls for detection of the 1.6 MeV gamma ray that accompanies the 40.2 hour half life beta decay of ^{140}La. The ^{140}La comes principally from the beta decay of the fission product ^{140}Ba that has a half-life of 12.8 days. After about 10 days following reactor shutdown, the ^{140}La density is proportional to the ^{140}Ba atom density and decays with the ^{140}Ba half-life. The ^{140}Ba fission product distribution is characteristic of the fission distribution or integrated power history over the last 5 half-lives or approximately 60 days of reactor operation. Thus, the scan results can be used to determine "recent" core power distribution. The 12.8-day half-life of ^{140}Ba also makes it imperative that the gamma scan data be collected as soon as possible after core shutdown, usually during refueling operations, since bundles with powers of interest are normally reinserted for additional use. Gamma ray spectral lines from other isotopes can be used for determination of plenum fission gas (^{85}Kr) or fuel exposure (^{137}Cs/^{144}Pr), but only power comparisons are the subject of this report.

A follow-on comparison of the measured ^{140}Ba distribution with predictions using the analytical tools of GNF (i.e. TGBLA/PANACEA) constitutes a validation of methods that can be used to support methods licensing or determination of other licensing uncertainties. The "Improved Steady-State Methods," also known as TGBLA06 / PANAC11, for core design, licensing, and core monitoring (Reference [1]) are the most widely used GNF methods, and this methodology is examined in this report. Additionally, comparisons between the gamma scan data and TGBLA04/PANAC10 (Reference [2]), an earlier design model, are provided in this report

As stated above, the output of the gamma scan measurement is the three dimensional ^{140}Ba distribution in the fuel. The process of converting the gamma detector response to ^{140}Ba distribution is described in Section 4 of this report. The nodal simulator is used to calculate the same ^{140}Ba distribution and the accuracy is determined by comparing the measured and calculated distributions. The nodal simulator process starts by providing the power/flow history of the core to the nodal simulator. The TIP predictions from the core tracking are compared to the measured TIP response for the first phase of the power distribution validation process. The power history over the last 60-90 days of operation is then integrated to generate the predicted nodal relative ^{140}Ba concentration.

At this point, a first examination is made of measured data. When using a detector to measure the ^{140}La gamma ray for rods still bound in the assembly, the natural source strength seen by the detector will be affected by the geometry of the lattice. Modern fuel types contain axial heterogeneity because of part length rods (PLR). Multiple bundle product lines may have differences in PLR arrangement and height

that must be accounted for in the interpretation of the measurement. Therefore, before a consistent comparison can be made, a third step must be made to correct the experimental node average ^{140}La intensity for physical (geometric) differences between fuel types to back-calculate the node average ^{140}Ba distribution.

The final step is to statistically compare the experimental and predicted ^{140}Ba predictions and explain the relationships on a radial (bundle) and nodal basis. This process may also be repeated using the measured 6" average TIP readings that can be input to the adaptive methodology described in References [3] and [4] for consistent confirmation of SLMCPR uncertainties.

2 *Plant and Fuel Description*

Cofrentes NPP is a high power density (52 kW/l) BWR/6 in Valencia, Spain that operated at 104.18% of original licensed thermal power for the period in which the current data were taken. The cycle 13 core was composed of a heterogeneous loading of multiple fuel types from multiple vendors, including GE11, GE12, and SVEA-96 product lines. The GEH product lines include part length rods. The core loading by bundle type is provided in Figure 2-1 while Table 2-1 provides more information on the total number of bundles loaded and batch average exposure. Contrary to common industry practice, fuel products from multiple vendors are loaded simultaneously. Figure 2-2 shows the power/flow history through Cycle 13. For purposes of establishing the correct isotopic history, the Cofrentes core has been tracked from initiation of Cycle 5 (1989).

Table 2-1 Fuel Composition of Cycle 13

Map IDs	Total Scanned	Bundle Names	Total Loaded	EOC Batch Avg. Exposure
1	5	[[	64	15370.3
2	5		64	15720.0
3	8		64	15006.2
8	6		40	38154.3
9	10		151	38659.4
12	7		108	28109.7
13	5		76	29051.2
14	--		8	42120.3
15	4	]]	49	41651.4

DRAFT

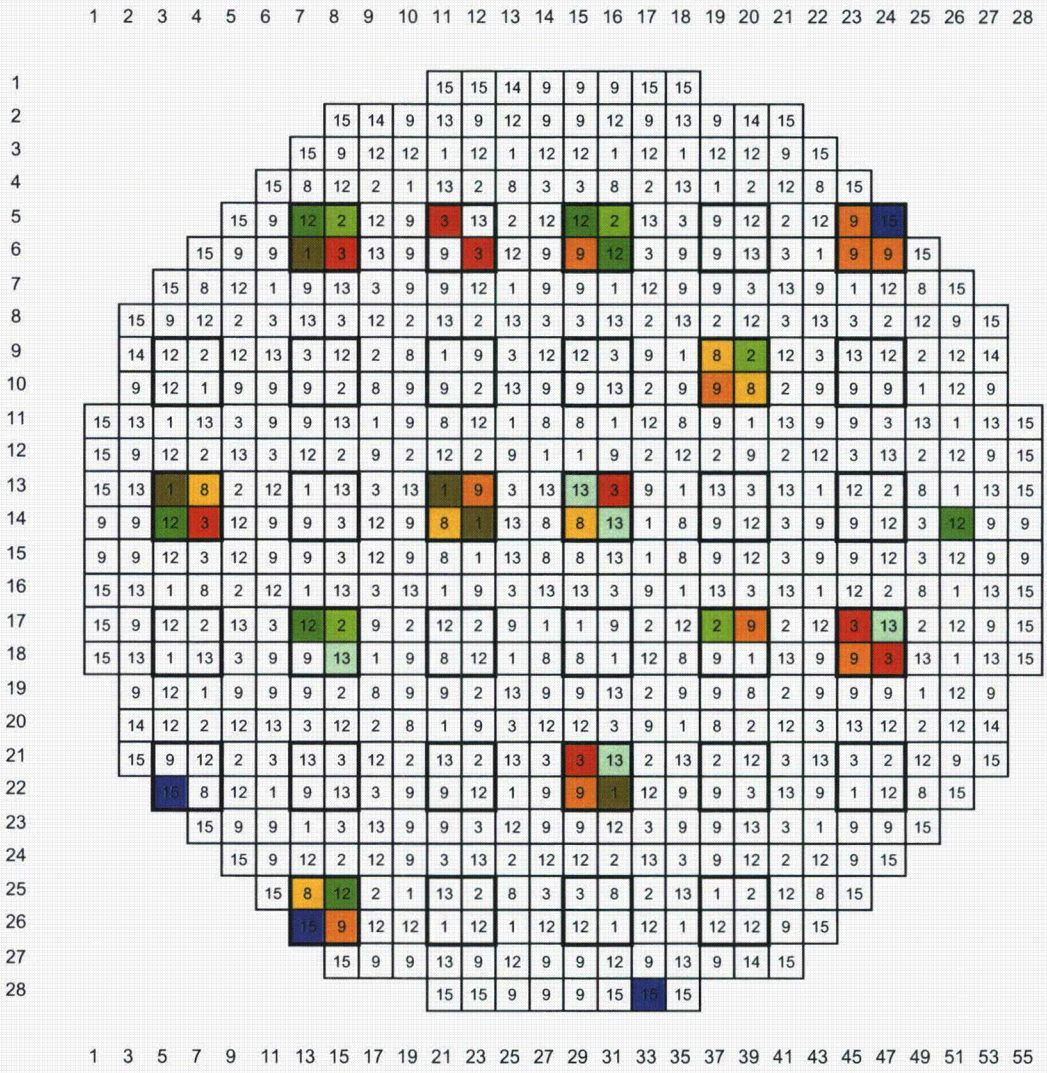

Figure 2-1 Cycle 13 Loading Pattern

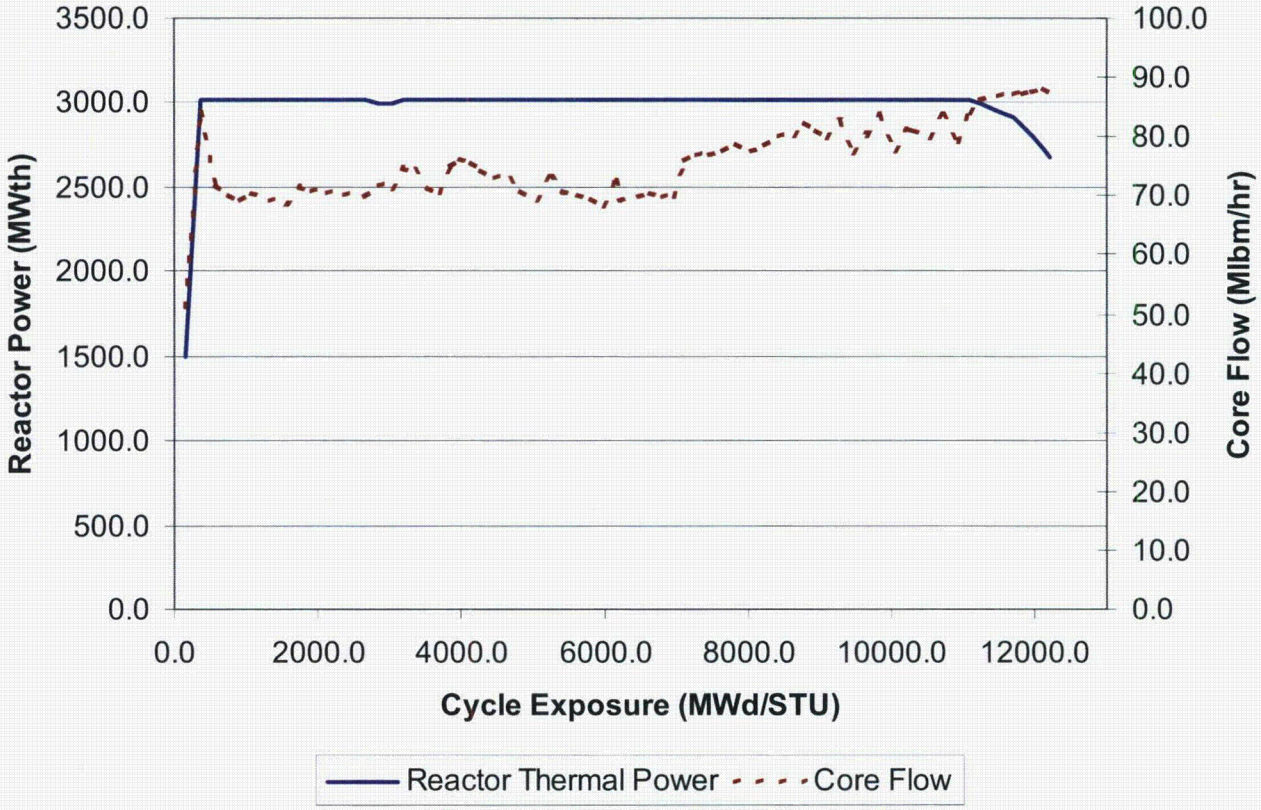

Figure 2-2 Cycle 13 Power/Flow History

3 *Traversing In-core Probe Comparisons*

3.1 Definition of Statistics

Three-dimensional power shape information as recorded by the Traversing In-core Probe (TIP) instrument readings can be compared to the calculated instrument readings from the simulator to determine its ability to calculate power distributions. Strings of either thermal neutron sensitive detectors (often referred to as thermal TIPs) or gamma-ray sensitive detectors (referred to as gamma TIPs) may be used to assess the normalized axial power shape along almost the entire length of the bundles within the four-bundle cell surrounding the instrument. The integrated signals may be combined to evaluate the radial power distribution within the core.

The 3D simulator models the response of the instrument to the appropriate particle species at the detector location to produce a simulated signal. For TIP comparisons, this simulated detector response is compared to the relative strength of the measured signal. TIP measurements are obtained periodically throughout an operating cycle to calibrate the fixed, in-core Local Power Range Monitors (LPRMs). The most common interval between TIP measurements is every 1000-2000 effective full power hours. During the time between TIP measurements the fast responding LPRMs are used to monitor the core power distribution. For a given TIP string, the measurement is a response to the integrated influence of the surrounding bundles. The signal strength from the fuel is primarily due to the cumulative power production of fuel rods in the four bundles surrounding the string.

The process for the TIP comparison basis is described below. The definitions of the quantities used in the calculations are:

$$P(k,j) = PCTIP(k,j)$$

$$C(k,j) = CALTIP(k,j)$$

$$I(j) = IFTIP(j)$$

$$S_j \Leftarrow j \in (I(j) = 0)$$

$$J = \#\text{ of elements in } S_j$$

$$K = Kup - Klow + 1$$

Klow, Kup = Node limits for axial comparison, usually 2 and 23

where

PCTIP(k,j) = the measured 6 in. average TIP reading in axial segment k of TIP string j

CALTIP(k,j) = the calculated 6 in. average TIP reading in axial segment k of TIP string j

IFTIP(j) = an indicator of when TIP readings are failed by the process computer, manually failed by the operator, or rejected by the core monitor for statistically poor performance

The measured and calculated TIP strings are normalized, respectively, as follows:

$$\sum_{j \in S_j} \sum_{k=Klow}^{Kup} P(k,j) = J \cdot K$$

$$\sum_{j \in S_j} \sum_{k=Klow}^{Kup} C(k,j) = J \cdot K$$

3.1.1 Nodal Statistic

The nodal RMS assesses all the predicted to measured instrument signals (for valid strings). Encompassing both radial peaking and axial structure, it is a global indicator of power shape agreement across the core for a given state point.

$$R_{nod} = \sqrt{\frac{\sum_{j \in S_j} \sum_{k=Klow}^{Kup} (P(k,j) - C(k,j))^2}{J \cdot K}}$$

The nodal statistic may also be reported for a given string.

$$\Delta_{j,nod} = \sqrt{\frac{\sum_{k=Klow}^{Kup} (P(k,j) - C(k,j))^2}{K}}$$

With this form, the nodal RMS becomes the following form.

$$R_{nod} = \sqrt{\frac{\sum_{j \in S_j} \Delta_{j,nod}^2}{J}}$$

3.1.2 Radial Statistic

The radial (or bundle) RMS assesses the string average predicted to measured instrument signals. In this way, the ability to predict the four-bundle average power uncertainty as applied in the SLMCPR process is assessed.

$$R_{rad} = \sqrt{\frac{\sum_{j \in S_j} \left(\left(\frac{\sum_{k=Klow}^{Kup} P(k,j)}{K} \right) - \left(\frac{\sum_{k=Klow}^{Kup} C(k,j)}{K} \right) \right)^2}{J}}$$

The bundle statistic may be reported for a given string and may be positive or negative.

$$\Delta_{j,rad} = \left(\frac{\sum_{k=Klow}^{Kup} C(k,j)}{K} \right) - \left(\frac{\sum_{k=Klow}^{Kup} P(k,j)}{K} \right)$$

With this form, the bundle RMS may be written in the following form.

$$R_{rad} = \sqrt{\frac{\sum_{j \in S_j} \left(\Delta_{j,rad} \right)^2}{J}}$$

3.1.3 Axial Statistic

The axial RMS assesses only the axial shape component of the predicted to measured instrument signals. The radial peaking between strings is normalized out for this comparison. Thus, it is a good indicator of the axial power shape agreement for the core state.

$$R_{axial} = \sqrt{\frac{\sum_{k=Klow}^{Kup} \left(\left(\frac{\sum_{j \in S_j} P(k,j)}{J} \right) - \left(\frac{\sum_{j \in S_j} C(k,j)}{J} \right) \right)^2}{K}}$$

The axial statistic may be reported for a given string if the string is first normalized unto itself.

$$P'(k,j) = \frac{\sum_{k=Klow}^{Kup} P(k,j)}{K}$$

$$C'(k,j) = \frac{\sum_{k=Klow}^{Kup} C(k,j)}{K}$$

$$\Delta_{j,axial} = \sqrt{\frac{\sum_{k=Klow}^{Kup} \left(P'(k,j) - C'(k,j) \right)^2}{K}}$$

3.2 TIP Summary

Radial, nodal and axial RMS statistics of the TIP comparisons are provided below as a function of cycle exposure for PANAC11 (Figure 3-1) and PANAC10 (Figure 3-2) for all TIP measurements through the cycle. These results, as well as calculated core average exit voids and maximum exit voids for any bundle, are in tabular form in Table 3-1. By inspection of the table, the exit void conditions are reflective of high power density BWRs in the United States and are immediately applicable. Cofrentes uses gamma sensitive TIP detectors.

Considering Figure 3-1, the results for PANAC11 are exceptionally good [[

]] As seen in Table 3-1, this accurate prediction is true even while the core average exit voids are generally around 75%, and the maximum exit void experienced during the cycle is 89%. Thus, the axial power shape and node-by-node power is accurately predicted throughout the core in the presence of significant void-quality profiles.

[[

]] At the point in the cycle of the highest exit void, details of the core average axial shapes and string-by-string details have been included in Figure 3-3 and Figure 3-4. It can be readily seen that the performance continues to be good at this point.

[[

]]. Since PANAC11 predicts the axial power more accurately throughout the cycle, it captures the depletion trajectory better and correctly predicts the power shift to the top near end-of-cycle.

Figure 3-5 through Figure 3-8 present PANAC11 axial comparisons for every TIP string and for the entire core at the last two TIP measurements. The performance here is excellent on both a core average and string-by-string basis even though the core flow is changing considerably between these two TIP runs. These two measurements occur within the window for the ^{140}Ba integration. Therefore, it will be useful to compare these to the results of the gamma scan data later in this report.

[[

]]

Figure 3-1 Summary of PANAC11 TIP Comparisons

[[

]]

Figure 3-2 Summary of PANAC10 TIP Comparisons

Table 3-1 Summary of PANAC10 and PANAC11 TIP Comparisons

Cycle Exposure (MWD/St)	Bundle RMS (%)		Axial RMS (%)		Nodal RMS (%)		Core Avg Exit Void (%)		Max Exit Void (%)	
	P11	P10	P11	P10	P11	P10	P11	P10	P11	P10
9.84	[[						64.5	64.2	74.8	74.7
248.43							72.8	72.6	82.4	82.6
763.25							76.1	75.9	86.6	86.5
1706.09							75.8	75.6	87.3	86.7
2861.80							75.5	75.3	87.1	87.1
3646.97							75.7	75.5	88.7	88.2
4503.98							75.0	74.8	89.0	88.4
5384.12							75.5	75.2	88.2	88.3
6411.31							75.7	75.5	88.3	88.5
6763.31							75.8	75.5	88.4	88.5
7439.08							73.9	73.6	86.6	86.7
8468.26							72.7	72.5	86.6	86.1
9278.40							73.8	73.5	86.5	86.1
10277.93							72.7	72.5	85.3	85.0
10393.16							73.1	72.8	85.5	85.2
11090.80							71.2	71.0	84.0	83.7
12121.01						]]	67.0	66.7	79.8	79.7

[[

]]

Figure 3-3 Core Average TIP for TIP dated April 9, 2001 (PANAC11)

[[

]]

Figure 3-4 Detail of TIP dated April 9, 2001 (PANAC11)

[[

]]

Figure 3-5 Core Average TIP for TIP dated January 7, 2002 (47 days prior to shutdown, PANAC11)

[[

]]

Figure 3-6 Detail of TIP dated January 7, 2002 (47 days prior to shutdown, PANAC11)

[[

]]

Figure 3-7 Core Average TIP dated February 19, 2002 (4 days prior to shutdown, PANAC11)

[[

]]

Figure 3-8 Detail of TIP dated February 19, 2002 (4 days prior to shutdown, PANAC11)

4 *Gamma Scan Comparisons*

4.1 Utilization of the Data for Power Distribution Benchmark

The gamma scanning technique measures the 1.596 MeV gamma-ray that accompanies the beta decay of ^{140}La. The primary mechanism for the accumulation of ^{140}La in exposed fuel is the beta decay of the fission product ^{140}Ba with a half-life of 12.79 days. Because of this equilibrium time constant, the ^{140}Ba distribution is characteristic of the integrated power history of the core during the last 2 to 3 months before shutdown.

Since the half-life of ^{140}La, 40.23 hours, is much shorter than that of, ^{140}Ba, following a period of approximately 10 days after shutdown, the ^{140}La activity is decaying at a rate determined by the half-life of ^{140}Ba and is proportional to the ^{140}Ba atom density.

The relationship between the production rate of ^{140}Ba (S_B) and fission density (F), at a time t, is given by

$$S_B = \left\{ \sum_k Y_{Bk} f_k \right\} F \quad , \quad \frac{Barium\ atoms}{cm^3 \sec}$$

where

Y_{Bk} = cumulative fission yield of Ba-140 from fissile nuclide k

f_k = fraction of fissions for fissile nuclide k

In the case of most fuels under consideration, the number of fissile nuclides, k, which contribute significantly to the fission rate, is small. Thus, we use

$$Y_e = effective\ yield = \sum_{k=1}^{4} Y_k f_k \Big/ \sum_{k=1}^{4} f_k \, , k = U-235, U-238, Pu-239 and\ Pu-241$$

To determine the total accumulation of Ba-140, then, requires solving the equation

$$\frac{dN_B(t)}{dt} = Y_e F(t) - \lambda_B N_B(t) \quad ,$$

where

N_B = Ba-140 atom density, atoms/cm^3

λ_B =Ba-140 decay constant = 0.05419 day^{-1}

Assuming that F is stepwise constant over the interval $\Delta t = t_n - t_{n-1}$ and equals to the average, therefore replacing the time integral with successive substitution, as

$$N_B(t_n) = \frac{Y_e(t_n) F(t_n)}{\lambda_B} + \left[N_B(t_{n-1}) - \frac{Y_e(t_n) F(t_n)}{\lambda_B} \right] \exp(-\lambda_B \Delta t)$$

4.2 Considering Geometrical Effects on the Gamma Scan

The measured gamma scan data supplied to GNF consists of nodal average values of measured detector signal intensity (pulses) of the 1596 keV gamma ray resulting from decay of ^{140}La. Each bundle was measured twice on all four corners for a total of eight measurements at 25 axial positions. These measurements were averaged together to determine the "node" value. The transmittal indicates that all measurement corrections (detector dead-time, drift, extent of measurements, etc.) have been applied. The detector intensity was provided in arbitrary units consistent for all assemblies. Figure 4-1 shows the general geometry of the gamma scan system.

[[

]]

Figure 4-1 Depiction of the fuel and collimator geometry (dimensions removed)

Since the lattices in these bundles were of differing type with differing water and part length rod locations, the geometric and material difference between each lattice type must to be taken into account when trying to normalize the collimator response to the 1596 keV ^{140}La gamma rays. The problem is analogous to geometric view factors used for radiative heat transport calculations. The MCNP Monte Carlo neutron transport code (Reference [5]) was used to simulate the explicit geometry for the purpose of characterizing the lattices on a relative basis. The gamma ray source terms for this simulation were taken from TGBLA06 pin power distributions for the nodal exposure and spectral history calculated by PANAC11. These correction (or inter-calibration) factors were used to re-normalize the measured collimator responses for the purpose of comparing the nodal simulator predictions to the measurements. However, this operation should not be considered experimental correction but rather another component of the analytical methodology prediction process.

4.3 Definition of Statistics and Process

The definition of the appropriate statistical population recognizes three important elements. First, bundles are often grouped by region, bundle type, or complete four-bundle cell. Second, the measured data had higher uncertainties on the lowest and two highest nodes. [[

]].

Measured and simulated data are normalized as follow:

$$\tilde{G}_k^n = G_k^n * \frac{\sum_{n=1}^{N} W(n) * K}{\sum_{n=1}^{N} \sum_{k=Klow}^{Kup} G_k^n * W(n)}$$

where,

G : raw barium density (measured or simulated)

$\tilde{G}$: normalized barium density (measured or simulated)

k : axial elevation index

n : scanned bundle index

N : total number of scanned bundles

Klow : minimum axial elevation used in the statistics

Kup : maximum axial elevation used in the statistics

K = Kup – Klow + 1

W(n) : weighting =1 if octant interior bundle without symmetric pairs in the gamma scan database

= 0.5 if bundle on a diagonal

= 1/L if bundle has L other symmetric bundles in the gamma scan database

The default option in the normalization process is to use the "octant" weighting option (=0), with the coefficients W(n) described above. The alternative is to use uniform weighting for every bundle (weighting option =1).

The bundle average data is calculated as follow:

$$G_b^n = \frac{\sum_{k=Klow}^{Kup} \tilde{G}_k^n}{K}$$

If g_i denotes the gamma scan data, p_i denotes the simulator prediction, and N defines the set of appropriate bundles, "SIGMA" and "RMS" denote the following relationship for nodal statistical comparisons.

$$d_{nk} = p_{nk} - g_{nk}$$

$$\bar{D} \equiv \frac{1}{K * N} \sum_{n=1}^{N} \sum_{k=Klow}^{Kup} d_{nk}$$

$$SIGMA = \sigma = \sqrt{\frac{1}{K * N - 1} \sum_{n=1}^{N} \sum_{k=Klow}^{Kup} (d_{nk} - \bar{D})^2}$$

$$RMS = \sqrt{\frac{1}{K * N} \sum_{n=1}^{N} \sum_{k=Klow}^{Kup} (p_{nk} - g_{nk})^2}$$

For nodal comparisons, the p_i and g_i denote nodal values over the valid axial positions (K_{low} to K_{up}) for bundles defined in the set. For bundle comparisons, a similar statistic is created where the delta is based upon difference between the average values from the valid axial positions for all bundles defined in the set. For axial comparisons, the comparison is exactly the same as the nodal comparison except that the bundle average bias is first normalized away from both strings so that the axial shape may be isolated and compared. The procedure for bundle and axial comparisons are analogous to the TIP statistical comparison procedure described in Section 3.1.2 and 3.1.3, respectively.

A description of the [[ ]] statistic is contained in Section 5.1.

4.4 Gamma Scan Comparison Summary

The final results using the basis defined above are summarized in Table 4-1. [[

]] This relationship is strong evidence that power distribution comparisons via TIP form a solid foundation for validation. Gamma scan measurements are not needed for validation on a frequent basis.

Table 4-1 Summary of Gamma Scan Comparison

Case	Output	Bundle		Axial		Nodal	
		RMS	SIG	RMS	SIG	RMS	SIG
1	[[						
2							
3							
4							
5							
6							]]

To improve axial power shape agreement during the core monitoring process, the shape adaptive methodology described in References [3] and [4] is applied. [[

]]

Figures 4-12 through 4-15 present the absolute difference in the bundle average ^{140}Ba (PANAC11 and PANAC10) on a radial map. Figures 4-16 through 4-19 present the relative difference (% error) in the bundle average ^{140}Ba (PANAC11 and PANAC10).

[[

]]

Figure 4-2 Comparison of Predicted vs. Measured Results (PANAC11)

[[

]]

Figure 4-3 Comparison of Predicted vs. Measured Results (PANAC10)

[[

]]

Figure 4-4 Error in Bundle Average ^{140}Ba versus Exposure (PANAC11)

DRAFT

[[

]]

Figure 4-5 Error in Bundle Average ^{140}Ba versus Exposure (PANAC10)

[[

]]

Figure 4-6 Error in Bundle Average ^{140}Ba versus Distance to Center (PANAC11)

[[

]]

Figure 4-7 Error in Bundle Average ^{140}Ba versus Distance to Center (PANAC10)

[[

]]

Figure 4-8 Error in Bundle Average ^{140}Ba versus Distance to Center (PANAC11, all bundles)

[[

]]

Figure 4-9 Examination for Trending versus Bundle Power (PANAC11)

[[

]]

Figure 4-10 Examination of Trending versus Axial Height (PANAC11)

[[

]]

Figure 4-11 Examination of Trending versus Axial Height (PANAC11, Adaptive)

[[

]]

Figure 4-12 Bundle Average ^{140}Ba Error (Δ, PANAC11, Adaptive) - Left

[[

]]

Figure 4-13 Bundle Average ^{140}Ba Error (Δ, PANAC11, Adaptive) - Right

[[

]]

Figure 4-14 Bundle Average ^{140}Ba Error (Δ, PANAC10, Adaptive) - Left

[[

]]

Figure 4-15 Bundle Average ^{140}Ba Error (Δ, PANAC10, Adaptive) - Right

[[

]]

Figure 4-16 Bundle Average ^{140}Ba Error (%, PANAC11, Adaptive) -Left

[[

]]

Figure 4-17 Bundle Average ^{140}Ba Error (%, PANAC11, Adaptive) – Right

[[

]]

Figure 4-18 Bundle Average ^{140}Ba Error (%, PANAC10, Adaptive) –Left

[[

]]

Figure 4-19 Bundle Average ^{140}Ba Error (%, PANAC10, Adaptive) –Right

5 // *//*

5.1 Definition of Statistics

[[

]].

Table 5-1 Summary of [[ ]] Comparisons

Case	Output	[[ ]]		Bundle	
		RMS	SIG	RMS	SIG
1	[[				
2					
3					
4					
5					
6					]]

As described in References [3] and [4], GEH's standard NRC approved Safety Limit Minimum Critical Power Ratio (SLMCPR) methodology utilizes an average uncertainty, [[ ]], of [[ ]]% for the [[

]]

5.2.1 PANAC10 Based [[ ]]

[[

]] The database for this collective gamma scan data is summarized in Table 5-2.

Table 5-2 Summary of Gamma Scan Measurements Using the PANAC10 3D Simulator

Plant and Cycle	[[	[[	New Fuel Geometry	Core Power Level (MWt)	Avg. Power Density (kW/l)
Hatch 1 EOC1			7x7	2436 (100%)	51.2
Hatch 1 EOC3			8x8 (C2) 8x8R (C3)	2436 (100%)	51.2
Quad Cities 1 EOC2			7x7 (C1) 7x7, 8x8 (C2) 7x7 MO_2 (C2)	2237 (100%)	36.4
Quad Cities 1 EOC4			8x8	2237 (100%)	36.4
Quad Cities 1 EOC5			8x8R	2237 (100%)	36.4
Millstone 1 EOC7			8x8R	1727 (100%)	35.0
Weighted Average[1]					
Cofrentes EOC13		]]	9x9 10x10 10x10 SVEA	2891 (100%)	52.4
Weighted Average[1]	]]				

[1] weighted $\sigma = \sqrt{\sum_{i=1}^{k}(n_i - 1)\sigma_i^2 \ /(\sum_{i=1}^{k} n_i - k)}$ where n_i = sample size for sample I

5.2.2 PANAC11 Based [[ ]]

[[

]] The database for this gamma scan data is summarized in Table 5-3.

[[

]]

Figure 5-1 [[ ]] (PANAC11, Adaptive) -Left

[1] Note that [[ ]]

[[

]]

Figure 5-2 [[ ]] (PANAC11, Adaptive) -Right

[[

]]

Figure 5-3 [[ ]] (PANAC10) - Left

[[

]]

Figure 5-4 [[ ]] (PANAC10) - Right

Table 5-3 Summary of Gamma Scan Measurements Using the PANAC11 3D Simulator

Plant and Cycle	[[	[[	New Fuel Geometry	Core Power Level (MWt)	Avg. Power Density (kW/l)
Hatch 1 EOC1			7x7	2436 (100%)	51.2
Hatch 1 EOC3			8x8 (C2) 8x8R (C3)	2436 (100%)	51.2
Weighted Average[1]					
Cofrentes EOC13		]]	9x9 10x10 10x10 SVEA	2891 (100%)	52.4
Weighted Average[1]	]]				

[1] weighted $\sigma = \sqrt{\sum_{i=1}^{k}(n_i - 1)\sigma_i^2 \ /(\sum_{i=1}^{k} n_i - k)}$ where n_i = sample size for sample i

6 *Conclusions*

The power distribution validation data available for Cofrentes Cycle 13 has been compared to the existing GEH/GNF simulator technology approved by the NRC. The results between the measurements and predictions using the TGBLA06 lattice physics code and the PANAC11 BWR core simulator are excellent with radial RMS errors less than 2% at bundle level and less than 4% at a nodal level. The results are consistent with the original SLMCPR analysis (Reference [3]), hence no changes to the SLMCPR uncertainties are needed for modern core and fuel designs or operational strategies. This is consistent with prior NRC communications on these subjects. In fact, considering the uncertainties derived from the data examined to date with the TGBLA06/PANAC11 methodology, the power distribution uncertainties could (potentially) be reduced from the current values applied in the SLMCPR analyses subject to regulatory approval. One should also observe that while the gamma scan campaigns yield information not available in the more common and routinely taken TIP measurements, the two validation data sets are wholly consistent.

7 *References*

[1] Letter from USNRC to G. A. Watford (GE), "Amendment 26 to GE Licensing Topical Report NEDE-24011-P-A, 'GESTAR II' - Implementing Improved GE Steady-State Methods," November 10, 1999.

[2] "Steady State Nuclear Methods," NEDE–30130–P–A, April 1985.

[3] "Power Distribution Uncertainties for Safety Limit MCPR Evaluations," NEDC-32694P-A, August 1999.

[4] "Advanced Methods Power Distribution Uncertainties for Core Monitoring," NEDC-32773P, Revision 1, January 1999.

[5] MCNP01A; General Electric version of MCNP4A, DRF J11-02538, March 1995. J. F. Briesmeister, "MCNP - A General Monte Carlo N-Particle Transport Code, Version 4A," LA-12625-M Manual, Los Alamos National Laboratory, (1993).

[6] Letter from J. S. Post (GE) to USNRC, Document Control Desk, "Part 21 Evaluation; Power Distribution Uncertainty Reassessment," MFN 05-082, August 18, 2005.

[7] GE Nuclear Energy, "Applicability of GE Methods to Expanded Operating Domains," NEDC-33173P, February 2006.